Quaternary Science Advances 3 (2021) 100021

Contents lists available at ScienceDirect

Quaternary Science Advances

journal homepage: www.journals.elsevier.com/quaternary-science-advances

High elevation ice patch documents Holocene climate variability in the northern Rocky Mountains

Nathan J. Chellman [a,b,*], Gregory T. Pederson [c], Craig M. Lee [d], David B. McWethy [e], Kathryn Puseman [f], Jeffery R. Stone [g], Sabrina R. Brown [h], Joseph R. McConnell [a]

[a] Division of Hydrologic Sciences, Desert Research Institute, 89512, USA
[b] Graduate Program of Hydrologic Sciences, University of Nevada, Reno, 89557, USA
[c] U.S. Geological Survey, Northern Rocky Mountain Science Center, 59715, USA
[d] Institute of Arctic and Alpine Research (INSTAAR), University of Colorado, 80309, USA
[e] Department of Earth Sciences, Montana State University, 59717, USA
[f] Paleoscapes Archaeobotanical Services Team, 80421, USA
[g] Department of Earth and Environmental Systems, Indiana State University, 47809, USA
[h] Department of Science & Mathematics, Defiance College, Defiance, OH, 43512, USA

ARTICLE INFO

Keywords:
Paleoclimate
Water isotopes
Ice core
Rocky mountains

ABSTRACT

Paleoclimate records from ice cores generally are considered to be the most direct indicators of environmental change, but are rare from mid-latitude, continental regions such as the western United States. High-elevation ice patches are known to be important archaeological archives in alpine regions and potentially could provide records important for Earth System Model evaluation and to understand linkages between climate and early human activities, but this potential largely is unexplored. Here we use a well-dated ice-core record from a shallow ice patch to investigate Rocky Mountain winter-season climate during the Holocene. Our records indicate that this ice patch consistently accumulated ice over the past 10 kyr, preserving a regionally representative climate record of stable water isotopes and ice accretion rates that documented generally cooler and wetter conditions during the early Holocene and 500 years of anomalous winter season warmth centered at 4100 cal yr BP followed by a rapid cooling and 1500 years of cooler and wetter winters.

1. Introduction

Recent climate warming has revealed important archaeological materials as alpine ice patches in the Rocky Mountains and worldwide recede, including artifacts more than 10,000 years old such as wooden hunting shafts, basketry, leather objects, and animal remains from hunting activities. Archaeologists postulate that these long-lived alpine ice patches served as refuges for wildlife and attracted the ancestors of Native Americans/First Nations peoples who left behind hunting implements and other cultural items, thereby providing archives of human and animal behavior in alpine settings throughout the Holocene (Dixon et al., 2014; Hare et al., 2012; Kuzyk et al., 1999; Lee, 2010, 2018; Lee and Puseman, 2017; Reckin, 2013). Although their archaeological significance is well-established, the potential for ice patches to provide ice-derived paleoclimate records has been largely unexplored.

Climate proxies spanning the complete Holocene from mid-latitude North America are limited primarily to lake-sediment cores (Anderson, 2011; Shuman, 2012; Shuman and Marsicek, 2016). Tree-ring based records of climate extend only over recent millennia (Pederson et al., 2011; Salzer et al., 2014), speleothem records from caves (Lundeen et al., 2013) are rare and often include long-lasting hiatuses, and glacial ice cores—generally considered to be the most direct records of environmental change—are limited to recent centuries (Beal et al., 2015; Chellman et al., 2017). Records from ice patches, however, have the potential to provide ice-derived proxies of Holocene climate from sensitive, high-elevation environments. These enigmatic features do not accumulate enough mass during cold, wet eras to develop into flowing glaciers, yet they persist on the landscape through warm, dry periods.

Here, we investigated the potential for ice patches to serve as paleoclimate archives by developing records of ice accumulation rate and stable water isotopes from a well-dated, 5.6-m ice core recovered from an ice patch on the Beartooth Plateau, Wyoming (Fig. 1) at an elevation of

* Corresponding author. Division of Hydrologic Sciences, Desert Research Institute, 2215 Raggio Parkway, Reno, NV, 89512, USA.
E-mail address: Nathan.chellman@dri.edu (N.J. Chellman).

https://doi.org/10.1016/j.qsa.2020.100021
Received 11 September 2020; Received in revised form 20 November 2020; Accepted 10 December 2020
Available online 15 December 2020

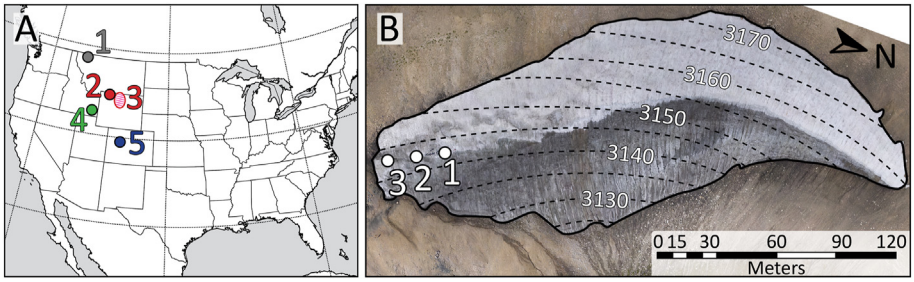

Fig. 1. Study sites. (**A**) Locations of selected proxy records discussed in text. Upper Kintla Lake (Site 1), Beartooth Plateau (Site 2; Beartooth ice patch, Emerald Lake, Beauty Lake, Island Lake), Bighorn Basin (Site 3), Minnetonka Cave (Site 4), and Bison Lake (Site 5). (**B**) Outline and aerial photo of the ice patch (Site 2) taken in August 2016, including the three coring locations (numbers correspond to cores as described in Methods) and elevation contours. [Aerial photo credit: J. Strait, Montana Department of Environmental Quality].

3145 m. A 10,000-year-old hunting-dart foreshaft previously recovered along the melting edge of this ice patch indicated the recent presence of early Holocene ice that was necessary to preserve the wooden artifact (Lee, 2010). In this study, we 1) discuss potential controls on ice patch formation and growth, 2) compare recent ice patch water isotope data to modern snowpack measurements, and 3) evaluate the ice patch accumulation and water isotopes records against established regional paleoclimate records from a speleothem and lake sediment cores—including the sediment accumulation rate from nearby Island Lake—to assess the paleoclimate significance of the ice patch records.

2. Materials and methods

2.1. Beartooth ice patch

Three ice cores were recovered from the Beartooth ice patch (elevation 3145 m; Fig. S1) located in the Shoshone National Forest, Wyoming in late August 2016. The closest meteorological monitoring site to the ice patch with modern observational data (1980 to present) is the Beartooth Lake SNOTEL site (United States Department of Agriculture, 2020) located ~10 km away at an elevation of 2850 m, approximately 300 m lower than the ice patch. The average annual precipitation at this site is 87 cm with a mean annual air temperature of −0.3 °C (Fig. S2). Average daily air temperatures range from −9 °C in winter (December, January, February) to 9 °C in summer (June, July, August). Mean daily temperatures are above 0 °C from early May to mid-October, with mean daily low and high temperatures above 0 °C from mid-June to early September and from early March to late October, respectively. Over the observational period, peak snow water equivalent (SWE) is reached around April 30th, and seasonal snow typically disappears by July 16th. By the peak SWE and snow disappearance dates, 68 ± 17% and 87 ± 17% (mean±1σ), respectively, of the average annual precipitation has occurred. Cool-season precipitation in the greater region is dominated by Pacific storms transported by westerly winter flow, while warm-season contributions are derived from moisture advected northward from the Gulf of Mexico, particularly in late spring and early summer (Wise et al., 2018).

The ice patch, referred to as ice patch TL1, faces northeast and is ellipsoidal in shape, having a 215-m horizontally oriented long-axis and 120-m short axis parallel to the underlying slope at the time of the coring (Fig. 1). The cores were recovered using a 4" electromechanical, two-barrel drill powered by a 2-kW generator (Kyne and McConnell, 2007). The lengths of the three cores were 5.61 m, 2.88 m, and 1.69 m, hereafter referred to as Cores 1, 2, and 3, respectively (Fig. S1). Cores 1 and 2 generally were of good quality, with most pieces longer than 30 cm. However, between 1.5 and 2.53 m in Core 2, we recovered small pieces less than 5 cm in length resulting in uncertainty in the orientation and order of the samples in this section. Core 3 was of poor quality, with many chips and re-drilled sections caused by partial recovery of previous drill runs that left ice in the borehole. Cores 1 and 2 were comprised of intact clean ice units bisected by organic-rich layers (Fig. S1). These layers were removed in the field using a hand saw and stored unfrozen in screw-cap plastic containers for further analysis. The clean ice units between organic-rich layers were bagged, immediately stored in the field in foam-insulated ice core boxes with dry ice, and transported frozen to the Desert Research Institute (DRI), Reno, Nevada.

To develop a depth-age scale, material from each of the 29 organic-rich layers in Core 1 was radiocarbon dated at the Laboratory for AMS Radiocarbon Preparation and Research (Boulder, CO; Table S1). We used the R-package Bacon v2.2 to calculate the radiocarbon age as calibrated year before present (cal yr BP, IntCal13) and to develop a depth-age model for the cores with associated uncertainties (Blaauw and Christen, 2011; Reimer et al., 2013; R Development Core Team, 2013). We calculated the net ice accumulation or accretion rate as the slope of the depth-age model.

The clean ice units were subsampled for discrete analysis. On average, samples were taken at 5-cm depth resolution, although resolution in some sections was a high as 2 cm to permit sampling between closely spaced organic-rich layers and as low as 8 cm in sections with poor ice quality. The frozen ice subsamples were rinsed with 18 MΩ ultrapure water, transferred to clean Whirlpak® bags, and melted at room temperature. The meltwater was transferred to 50 ml polypropylene vials, sonicated for 10 min, and subsequently analyzed for water isotopes ($\delta^{18}O$, δD). Measurements were made within 8 h of melting using a Picarro 2130i (Picarro Inc., Santa Clara, CA) calibrated to Vienna Standard Mean Ocean Water (VSMOW). To prevent clogging during sample introduction, the meltwater was filtered with an inline 20 μm stainless steel filter. Two pieces of organic material found within the upper clean ice units were collected and radiocarbon dated at the National Ocean Sciences Accelerator Mass Spectrometry facility (Woods Hole, MA; Table S2). A leaf recovered at a depth of 2.08 m was radiocarbon dated to either coincident with or slightly younger than the underlying organic-rich layer, while a twig identified at a depth of 0.22 m was modern carbon, indicating it was deposited during recent centuries.

Cores 2 and 3 were synchronized to an equivalent-Core 1 depth to facilitate comparisons of water isotope measurements. Assuming lateral continuity in the organic-rich layers, Core 2 was synchronized to Core 1 using the uppermost six organic-rich layers as tie points. Because only one organic-rich layer was recovered in the shallower Core 3 and overall ice quality was poor, Core 3 was visually synchronized to Core 1 using the water isotope profile.

2.2. Island Lake

A 1.5 m-long lake sediment core was recovered in July 2013 from the central basin of Island Lake (46.949 °N 109.543 °W; 2904 m) using a Griffith corer (Brown et al., 2020). We developed a depth-age model using the R-package Bacon v2.2 and eight extracted pollen samples radiocarbon dated at the Accelerator Mass Spectrometry Lab at directAMS and calibrated using IntCal13 (Blaauw and Christen, 2011; Reimer et al., 2013; R Development Core Team, 2013) (Fig. S3; Table S3). We calculated the sediment accumulation rate as the slope of the depth-age model.

3. Results

3.1. Ice patch chronology

Linking past changes in paleoclimate proxies to human history and records from other natural archives requires robust, accurate, and independent dating (Buntgen et al., 2011; deMenocal, 2001; Kuper and Kropelin, 2006). Unlike cores from polar ice sheets and alpine glaciers consisting only of clean ice, the cores recovered from the Beartooth Plateau ice patch were comprised of clean ice units bisected by distinct, organic-rich layers containing plant remains, animal dung, and soil that were used to develop a robust depth-age chronology for the ice cores.

A total of 29 organic-rich layers were found in the 5.6-m ice core (Fig. 2; Fig. S1), with each layer ranging in thickness from 0.2 to 4 cm. Because traditional ice-core dating techniques such as volcanic synchronization or annual layer counting were not applicable, we constrained the ages of the ice units using ^{14}C-derived ages of intact organic material selected from the organic-rich layers between the ice units. The depth-age scale had an average uncertainty of ±152 years (±2σ) (Fig. 2), and all but two of the 29 calibrated radiocarbon ages were in chronological order within their associated age uncertainties.

The deepest organic-rich layer was radiocarbon dated to between 10,258 and 10,444 cal yr BP (2σ uncertainty of calibrated age)—consistent with the 10,400 cal yr BP age of the wooden hunting-dart foreshaft recently recovered at the site (Lee, 2010)—demonstrating that the ice patch has persisted for more than 10,000 years. The continuity of the radiocarbon dates indicates largely uninterrupted ice accretion throughout the Holocene. The depth-age chronology shows a marked change at 3560 (3410 to 3880) cal yr BP (median and 95% confidence interval of modeled age scale; Fig. 2) when the average net ice accretion rate more than doubled from 0.02–0.04 cm yr^{-1} to 0.04–0.12 cm yr^{-1} (Fig. 3). Organic-rich layers formed at a frequency of 315 ± 235 (±2σ) years with no consistent relationship to the centennial-scale, climate-related water isotope records presented here, although layer formation on finer time scales may be related to extended warm, dry periods.

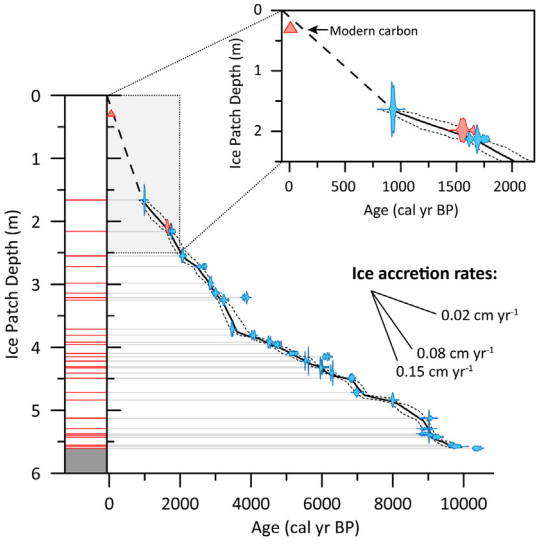

Fig. 2. Beartooth Plateau ice-core profile and chronology. 29 organic-rich layers (left, red lines) were identified in the 5.6 m-long core and their respective radiocarbon ages used to develop a chronology. Modeled age (black solid line) with 95% confidence intervals (black dotted lines). Dashed line indicates uncertainty in age from the uppermost organic-rich layer (1.6 m) to the surface. Radiocarbon dates (blue) derived from Bayesian depth-age modeling (Blaauw and Christen, 2011) have ranges in calibrated age shown as horizontal extents and age probabilities shown as vertical extents. Radiocarbon dates shown in red were extracted from a clean ice unit, not an organic-rich layer, and not included in the age model. Inset shows detail for the most recent two millennia.

3.2. Stable water isotopes

In Core 1, water isotopes (δ^{18}O) ranged from −16 to −24‰ (Fig. 3). δ^{18}O values were relatively steady from 10,000 to 7000 cal yr BP at −19‰, before a slight decrease to −20.5‰ at 7000 cal yr BP and increase to −16‰ from 4200 to 4000 cal yr BP. After this maximum, δ^{18}O values rapidly declined, remaining between −20 and −24‰ until 2000 cal yr BP before increasing to values between −16 and −19‰ over the most recent millennia. δ^{18}O values between three parallel cores were in good agreement, indicating similar depositional processes across the surface of the ice patch (Fig. S4).

3.3. Island Lake chronology

The oldest radiocarbon date for the Island Lake depth-age scale dated to 10,369 to 10,785 cal yr BP (2σ uncertainty of calibrated age), and the chronology had an average uncertainty of ±333 years (±2σ) (Fig. S3). The Island Lake sediment accumulation rate averaged 0.014 cm yr^{-1} from 10,500 to 9200 cal yr BP before decreasing to an average of 0.008 cm yr^{-1} from 9200 to 4400 cal yr BP. The accumulation rate more than doubled to an average of 0.029 cm yr^{-1} from 4400 cal yr BP until present.

4. Discussion

4.1. Processes of ice patch formation and growth

Current understanding of the processes underlying ice-patch formation and growth is limited and the same processes may not be applicable to all ice patches, potentially complicating the interpretation of ice-patch paleoclimate records. Thin, non-flowing ice patches are fundamentally different from much thicker glaciers and ice sheets that flow under their own mass. For the latter, precipitation accumulating as snow on the surface in higher elevation regions of positive surface mass balance is compressed and transported by ice flow to lower elevation regions of negative surface mass balance, leading to distortion and thinning of layers within the ice that increases with depth. This flow, along with basal melt of the bottommost ice at many sites, results in continual replacement or loss of the oldest ice. Hence while long, intact paleoclimate records can be recovered from the upper sections of thick ice sheets, most records from relatively thin alpine glaciers are limited to the past few centuries (Beal et al., 2015; Chellman et al., 2017).

All evidence, however, indicates that the Beartooth ice patch never flowed. First, the shallow, 5.6 m depth of the ice patch means that it is much too thin to flow under its current mass. Second, the ice patch is not located in a cirque headwall but located near the top of a ridge with the entire ice patch spanning just 50 m of vertical elevation and with similar slope and aspect (Fig. 1), so there are no distinct accumulation or ablation regions. Thus, the entire ice patch either is in positive or negative surface mass balance depending on year-to-year changes in local climate conditions. Third, the stratigraphy of the organic-rich layers within the ice patch is intact as indicated by coherent layers between multiple parallel cores (Fig. S1). Fourth, the organic-rich layers are distinct and not distorted or mixed with surrounding ice throughout the core, indicating the internal structure of the ice patch, even at the bottom, has not been deformed by movement. The lack of flow features throughout the core also suggests that the ice patch is not a remnant of a once-larger, now-retreated glacier.

Instead of processes that preserve accumulating snowfall, including debris or other impurities, on or near the surface of glaciers and ice sheets, ice accumulation most likely occurs at depth at the interface between the existing ice surface and overlying seasonal snow (Fig. 4), similar to processes suggested by previous studies of ice patches in the Northwest Territories (Meulendyk et al., 2012). During periods of positive annual surface mass balance on the ice patch, thin layers of ice are accreted approximately annually when percolating surface meltwater

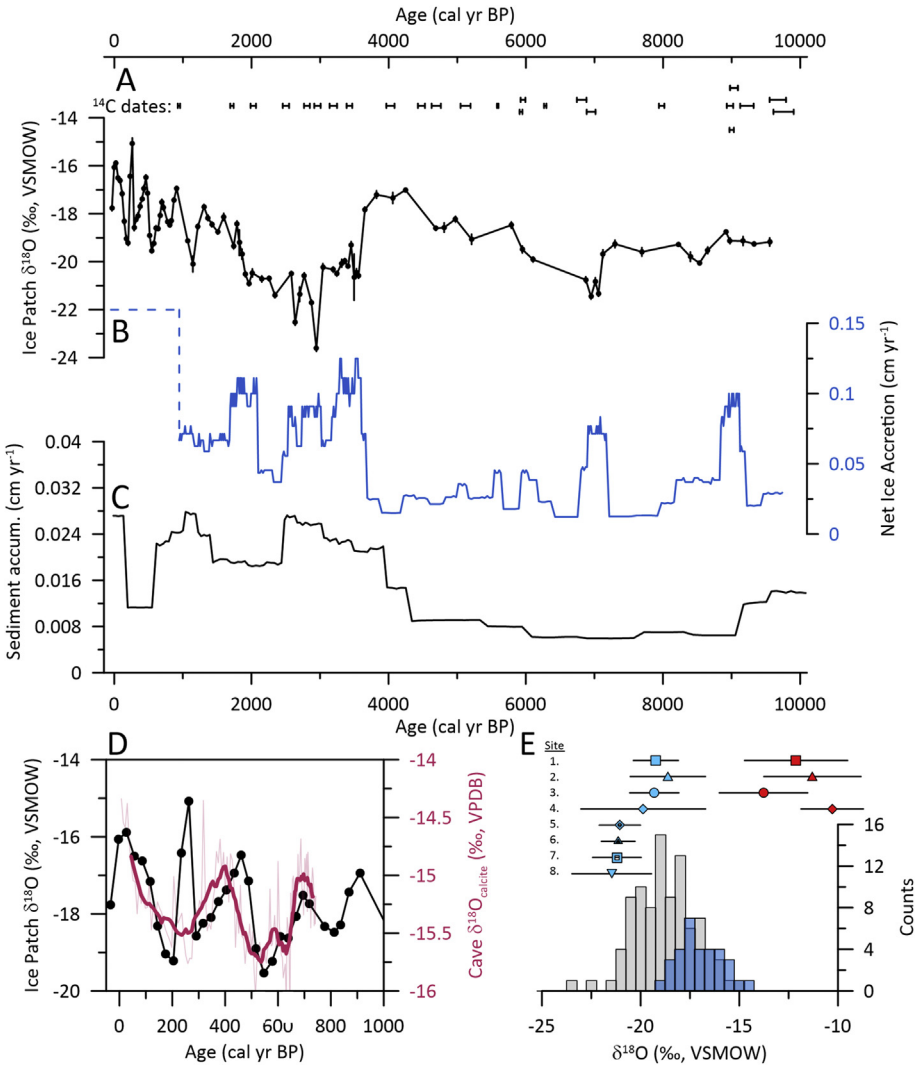

Fig. 3. Paleoclimate data from the Beartooth Plateau ice patch and Island Lake. (**A**) Calibrated ice-patch radiocarbon dates (2σ ranges) and $\delta^{18}O$ record (black). Vertical error bars represent 1σ analytical uncertainty of $\delta^{18}O$ measurements. (**B**) Ice patch net ice-accretion rate (blue). Dashed line to first age control point indicates uncertainty in current mass balance. (**C**) Island Lake sediment-accumulation rate. (**D**) Detail of ice patch (black) and Minnetonka Cave (Lundeen et al., 2013) (red with 11-point running average) comparison over past millennium. (**E**) Histogram of ice patch $\delta^{18}O$ data for the entire record (grey) and past 1000 years (blue) with modern isotopic values for cold- (blue) and warm-season (red) precipitation for 8 sites in Wyoming, Montana, and Idaho (Table S4).

reaches the interface between the cold, impermeable existing ice surface and the porous overlying seasonal snow cover. This meltwater is refrozen either early in the melt season while the ice patch retains the previous winter's cold temperatures or at the end of the season with the onset of freezing wintertime temperatures (Fig. 4). This proposed mechanism for ice accretion requires the presence of an overlying snowpack above the ice patch to provide a source of meltwater, to filter percolating meltwater, and to retain water at the snow-ice interface where it can refreeze (Fig. 4).

Support for this hypothesis comes from the clarity of the preserved ice, as well as its isotopic composition. The clean ice units are nearly completely devoid of any debris, consistent with preservation of filtered meltwater, in contrast with preservation of residual seasonal snow that would include both entrained and surface debris. This mechanism implies that any isolated debris entrained within an ice unit was deposited coeval with the seasonal snow during the winter accumulation season and deposited immediately after the formation of an organic-rich layer by an extended period of negative surface mass balance. The radiocarbon date of a leaf recovered at a depth of 2.08 m—one of the few pieces of debris identified within a clean-ice unit—dated to either coincident with or slightly younger than the underlying organic-rich layer and so is consistent with this hypothesis.

4.2. Controls on ice core $\delta^{18}O$ and accumulation

Modern observations from the Beartooth SNOTEL site indicate that annual precipitation on the Beartooth Plateau is dominated by wintertime precipitation. Total accumulation at peak SWE and snow disappearance dates averages 68 ± 17% and 87 ± 17% (mean±1σ; Fig. S2), respectively, and 33 ± 16% of precipitation accumulating between these dates is associated with measurable increases in snow depth, indicating that snowfall events occur well into summer at this high elevation site. Though the observational data from the SNOTEL site, which is 300 m lower in elevation and 10 km away from the ice patch, are not directly translatable to the ice patch, these data imply that most precipitation falls as snow at the ice patch. Furthermore, snow drifting onto the ice patch would further enhance snow deposition relative to warm-season precipitation.

Values of $\delta^{18}O$ measured in the Beartooth ice patch are consistent with preservation predominantly of cool-season (October to May; used interchangeably with wintertime throughout the text) precipitation, most likely meltwater derived from the overlying seasonal snow with smaller contributions from warm-season (June to September) precipitation. Values of $\delta^{18}O$ varied from −16 to −24‰ (−19.0 ± 1.5‰; mean±1σ) over the Holocene and from −16 to −20‰ (−17.7 ± 1.1‰) over the past millennium (Fig. 3). These were comparable to reported

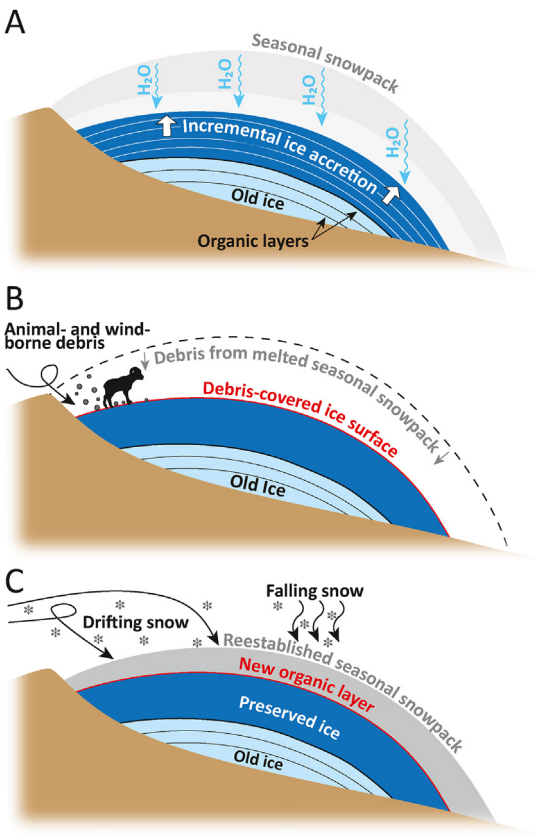

Fig. 4. Schematic diagram of ice patch (not to scale). (**A**) Ice accretion phase, when percolating meltwater is refrozen to the ice patch leading to incremental ice accretion. (**B**) Organic-rich layer formation, when melt of the overlying snowpack concentrates debris from the snow as well as externally deposited debris onto the ice patch surface. (**C**) Drifting-enhanced deposition of seasonal snow preserves organic matter as a distinct layer and ice accretion resumes.

$\delta^{18}O$ values from ice cores in the nearby Wind River Range (−15 to −22‰; −16.4 ± 1.4‰) extending back 250 years (Chellman et al., 2017; Naftz et al., 2002) and modern measurements of $\delta^{18}O$ in October through April precipitation from regional, high-elevation monitoring sites located 40–350 km from the ice patch (−17 to −24‰) (Anderson et al., 2016b; Benjamin et al., 2004; Vachon et al., 2007) (Fig. 3). The ice patch $\delta^{18}O$ values also are significantly lower than modern nearby measurements of summer precipitation (−9 to −17‰) (Benjamin et al., 2004; Vachon et al., 2007) (Fig. 3). The agreement of the ice patch stable isotopes ($\delta^{18}O$, δD) with the Global Meteoric Water Line (Craig, 1961) suggests little impact from post-depositional processes such as evaporation, and consistency of $\delta^{18}O$ values between three parallel cores from the ice patch indicates that preservation was spatially coherent (Fig. S4).

While there are numerous lake sediment $\delta^{18}O_{calcite}$ from the Rocky Mountains—including from nearby Crevice Lake in Yellowstone National Park (Whitlock et al., 2012)—lake sediment $\delta^{18}O_{calcite}$ records can integrate signals associated with basin hydrology including residence time, evaporation, and groundwater flow, and thus may not be primarily sensitive to meteoric precipitation inputs (Anderson et al., 2016a). Therefore, we evaluated the ice-patch $\delta^{18}O$ record against the $\delta^{18}O$ of calcite ($\delta^{18}O_{calcite}$) from the well-dated Minnetonka cave record in southeastern Idaho, previously interpreted to be a record of the isotopic composition of wintertime precipitation (Lundeen et al., 2013) (Figs. 1, 3, 5, S5). To our knowledge, this is the closest isotopic record to the ice patch that is thought to primarily reflect the isotopic signature of meteoric precipitation.

Comparisons to this speleothem record suggest that during periods of positive annual surface mass balance, ice accumulation appears to have been a continuous, incremental process. Although the speleothem record is not continuous throughout the Holocene because of hiatuses from either wet or cold wintertime conditions, and the speleothem also exhibits lower isotopic variability, likely related to smoothing from warm-season precipitation and the imprint of the mean annual cave temperature on the isotopic record (Lundeen et al., 2013), the overall trend of $\delta^{18}O_{calcite}$ closely paralleled the ice-patch $\delta^{18}O$ record for the continuous periods (e.g., 7500 to 4000 cal yr BP), and during the most recent 800 years when there is no evidence of extended melt events in the ice patch record. Temporal variations in the overlapping sections of the two records are also in close agreement, suggesting continuity of ice accretion at the ice patch.

Despite climate conditions that have driven numerous large-scale retreats and advances of alpine glaciers throughout the Holocene (Denton and Porter, 1970; Solomina et al., 2015) and modern retreat of glaciers in nearby areas (Berger, 2010; Hall and Fagre, 2003), the uniformity of the ice patch chronology implies that the Beartooth ice patch not only endured, but also consistently accreted ice through many climate states. The topographic setting of the ice patch undoubtedly was a factor buffering the ice patch from past climate extremes, as its aspect and location at the edge of a plateau ensured that a significant snowpack crucial for insulating the ice patch accumulated even during drier winters. Reliable accumulation from drifting also was important for rapid reestablishment of the overlying snowpack following prolonged periods of negative surface mass balance that would have exposed the surface of the ice patch and formed a new organic-rich layer (Fig. 4). These periods of negative annual surface mass balance concentrated matter from melting snow and ice, along with windblown or animal-borne debris, onto the ice-patch surface that was buried and preserved as a distinct organic-rich layer when positive mass balance resumed (Fig. 4). Though the formation of such layers required a brief hiatus in ice accretion, therefore precluding preservation of a temporally continuous ice record, it is unlikely the hiatuses were long-lived given that the shallow ice patch could not survive prolonged periods of negative mass balance without completely melting and the temporal consistency of the ice accretion rate chronology implies relatively continuous growth.

Developing a comprehensive, physically based understanding of the processes that govern the Beartooth Plateau ice patch isotopic and ice accretion records is difficult. Large seasonal variability observed at the ice patch impedes reliable monitoring or process-level studies of ice accretion at the ice-snow interface on multi-year timescales. For example, the ice-patch surface, exposed during the initial coring in autumn 2016 CE, was buried beneath 8 m of seasonal snow during coring attempts near the end of the autumn melt season in 2018 CE, after only two winters of above average snowfall. Limited access to the remote, high-elevation field site during winter and spring, when accumulation occurs, further complicates monitoring efforts.

4.3. *Ice patch paleoclimate implications*

We used the ice-accretion rate and $\delta^{18}O$ record from the ice patch, in conjunction with the precipitation-sensitive sediment accumulation rate from nearby Island Lake (Fig. 3, Fig. S3), to develop a record of local to regional Holocene climate. A number of physical processes may influence the $\delta^{18}O$ record preserved in the ice patch, including atmospheric circulation (Thompson et al., 2013), site temperature (Naftz et al., 2002), and seasonal biases in preservation (Fisher et al., 1983). Large-scale atmospheric circulation patterns have been linked to water isotope variability in modern precipitation (Welker, 2012), but model simulations show Holocene wintertime $\delta^{18}O$ changes of ~0.5–1‰ (Liu et al., 2014), much less than the observed ~4‰ variability, suggesting temperature and preservation biases are strong contributors to the $\delta^{18}O$ signal. Lacking a precise understanding of how these individual processes quantitatively contribute to the preserved $\delta^{18}O$ record, we consider the ice patch $\delta^{18}O$ to be a qualitative indicator of cool-season or wintertime

intensity with low $\delta^{18}O$ values representing either colder winters and/or enhanced snowfall leading to greater deposition and preservation of snow relative to warm-season precipitation.

The ice accretion rate at the ice patch, derived from the well-constrained chronology, is itself a paleoclimate indicator. The ice accumulation rate in the ice patch is not affected by ice thinning with depth, as the ice patch at only 6 m deep is too shallow to have internal flow that would result in thinning. Similar to findings based on cirque glaciers in Rocky Mountain National Park (Hoffman et al., 2007), we posit that ice accretion was more sensitive to temperature than precipitation, since the observed ice-accretion rates of less than 0.12 cm yr^{-1} required only minimal seasonal snow accumulation and the topographic setting of the ice patch at the edge of a plateau ensured sufficient accumulation from drifting even in drier winters. Thus, we assume that the ice-accretion rate was indicative of overall temperature, with cooler climates associated with increased ice accumulation.

Beginning 10,000 years ago, $\delta^{18}O$ values were relatively stable until ca. 7000 cal yr BP, suggesting little variation in winter conditions (Fig. 5). A brief increase in ice accumulation rate at 9100 (9040 to 9280) cal yr BP reflected cooler overall temperatures. This elevated ice accumulation rate coincided precisely with a hiatus in speleothem growth in Minnetonka Cave, attributed to cooler or wetter conditions (Lundeen et al., 2013). At 7140 (6960 to 7250) cal yr BP, a short-lived decrease of $\delta^{18}O$ to −21‰ and an increased ice-accretion rate indicate a brief era of relatively severe winter conditions, which preceded gradual wintertime warming until 4230 (4060 to 4380) cal yr BP when $\delta^{18}O$ reached a local maximum of −17‰. This interval of wintertime warming paralleled Northern Hemisphere pollen-derived temperature reconstructions that suggest a mid-Holocene climate optimum (Marsicek et al., 2018). Between ca. 4200 and 3800 cal yr BP, higher $\delta^{18}O$ values and low ice accretion rates indicated conditions in the region were the warmest of the Holocene with the mildest winters prior to the last millennium. This era coincided with widespread aridity at 4200 cal yr BP recorded worldwide in a range of proxies, including from western North America (Carter et al., 2018), as well as warm temperatures and dry conditions indicated by the Minnetonka Cave speleothem record (Lundeen et al., 2013).

Between 3930 (3730 to 4080) and 3560 (3410 to 3880) cal yr BP, the ice-patch records showed a rapid transition to cooler conditions and strong winters, evidenced by the synchronous decline in $\delta^{18}O$ values to between −21‰ and −24‰ and doubling of the net ice accretion rate in the ice patch, as well as a comparable increase in sedimentation rate in Island Lake (Fig. 3). At this time, a depositional hiatus attributed to cooler or wetter winters occurred in Minnetonka Cave (Lundeen et al., 2013) speleothem growth, and the diatom-inferred stratification index (DI-SI) for Emerald and Beauty Lakes—located 6 km and 10 km away, respectively, from the ice patch in the Beartooth Mountains—as well as Upper Kintla Lake in Glacier National Park, showed a rapid transition to more positive values indicating deeper mixing (Fig. 5) (Stone et al., 2016). Previous work had linked the shift to deeper lake mixing at Emerald, Beauty, and Upper Kintla lakes to a weakened Aleutian Low (Stone et al., 2016), which can result in enhanced winter storm activity and increased cool-season precipitation in the Rocky Mountains (Overland et al., 1999).

Around this time, changes are also noted in two North American lake-sediment $\delta^{18}O_{calcite}$ records thought to predominantly represent precipitation-$\delta^{18}O$ with minimal influence from other processes (Anderson et al., 2016a): the Bison Lake calcite $\delta^{18}O$ record indicated a shift from rain-to snow-dominated winter precipitation in Colorado (Anderson, 2011), while a transition in the $\delta^{18}O_{calcite}$ from Jellybean Lake in Alaska indicating a weakening Aleutian Low (Anderson et al., 2005) (Fig. 5). Additionally, cooler temperatures were recorded in lakes in Wyoming and North Dakota ca. 3000 cal yr BP (Shuman, 2012; Shuman and Marsicek, 2016). Moreover, this 1500 year cold and wet period coincided with glacial advances in the Canadian Rockies during the Neoglacial (Menounos et al., 2009; Osborn and Karlstrom, 1988) and highstands among many Utah and Nevada lakes in the Great Basin during the

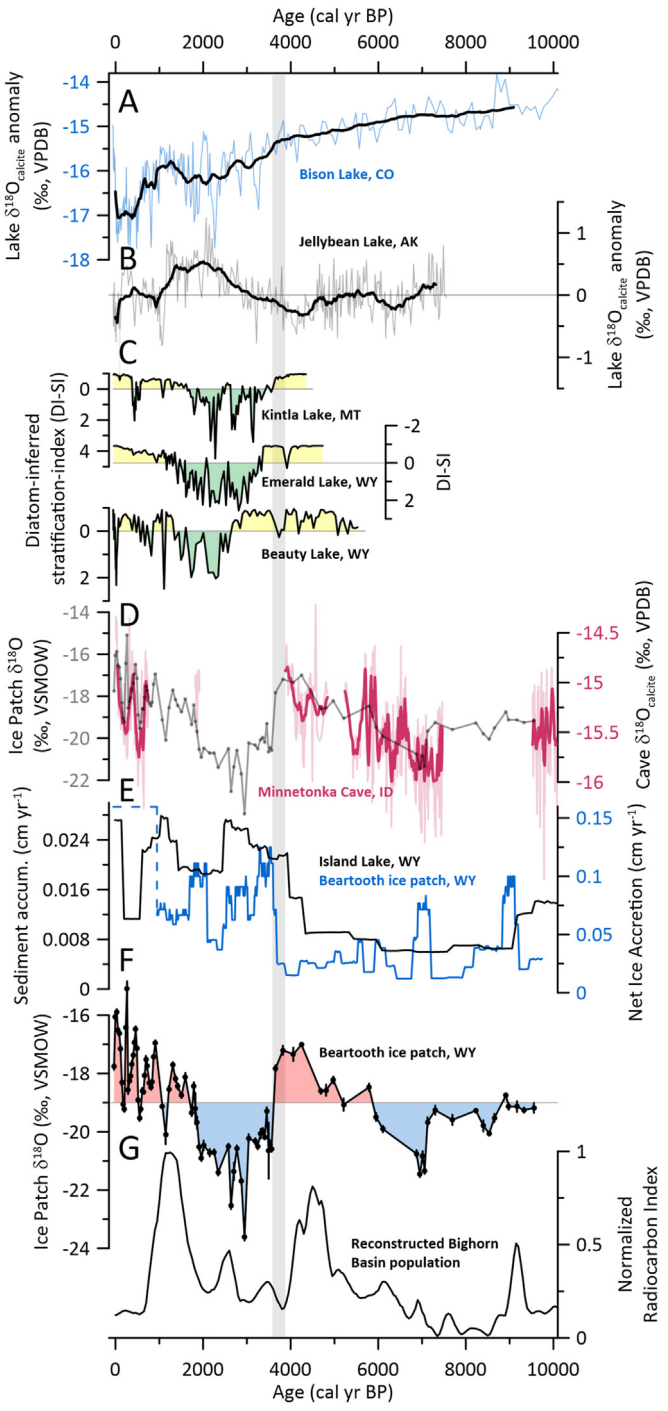

Fig. 5. Comparison of ice patch records to other proxy records. Grey vertical bar indicates timing of rapid decline in ice patch $\delta^{18}O$ values. (**A**) $\delta^{18}O_{calcite}$ from Bison Lake, CO (Anderson, 2011) (blue) with 21-point running average (black). (**B**) $\delta^{18}O_{calcite}$ from Jellybean Lake, AK (Anderson et al., 2005) (grey) with 21-point running average (black). (**C**) Diatom-inferred stratification-index (DI-SI) from Kintla Lake (Glacier NP, MT), Emerald and Beauty Lakes (Beartooth Mountains, WY) (Stone et al., 2016). (**D**) Minnetonka Cave speleothem $\delta^{18}O$ record (Lundeen et al., 2013) (red with 11-point running average) and ice-patch $\delta^{18}O$ (grey). (**E**) Island Lake sediment accumulation rate (black) and Beartooth ice patch net ice accretion rate (blue). (**F**) Beartooth ice-patch $\delta^{18}O$ record. (**G**) Normalized radiocarbon index for the Bighorn Basin (Kelly et al., 2013) (black).

Neopluvial (Yuan et al., 2013). Increased late Holocene moisture also has been noted in other lake-sediment records, including from Rainbow Lake on the Beartooth Plateau, though the timing of such increases varies across geographic regions (Shuman and Marsicek, 2016; Shuman and Serravezza, 2017).

Values of $\delta^{18}O$ in the ice-patch record remained relatively low until 2050 (1970 to 2240) cal yr BP, with relatively high ice- and sediment-accumulation rates in the ice patch and Island Lake, respectively, suggesting a prolonged era of cooler and more intense winters. This era is distinct in the ice-patch $\delta^{18}O$ record, with rapid transitions of greater than 3‰ bracketing 1500-years of below-average values. These conditions ended with an abrupt $\delta^{18}O$ increase from −21‰ to −18‰ between 2050 (1970 to 2240) and 1690 (1610 to 1780) cal yr BP followed by a gradual increase to modern levels between −16‰ and −19‰, indicating a wintertime warming trend during the past millennium in close agreement with Minnetonka Cave (Lundeen et al., 2013) (Fig. 3, Fig. S5). The increasing $\delta^{18}O$ also paralleled decreasing $\delta^{18}O_{calcite}$ at Jellybean Lake and decreasing DI-SI at Emerald, Beauty, and Upper Kintla Lakes, indicating less wintertime precipitation in the region and a strengthened Aleutian Low, respectively.

4.4. Linkages to regional human activity

The climate variability preserved in the ice patch paralleled Native American activity as inferred from radiocarbon dates on archaeological materials in the nearby Bighorn Basin for most of the Holocene (Fig. 5) (Kelly et al., 2013). A major decline in human activity in the region beginning between 4500 and 4000 cal yr BP (Kelly et al., 2013; Zahid et al., 2016), a trend not evident in other regions of North America (Peros et al., 2010), coincided with the onset of the warmest winter temperatures indicated in the ice-patch record during the mid-Holocene (Fig. 5). Indicators of human activity remained low during the unusually cold, wet Neoglacial period suggesting that such conditions also may have inhibited human activity in the Bighorn Basin, which is at odds with the previous interpretation that cool and wet periods fostered population growth (Kelly et al., 2013). Activity did not increase until ca. 2000 cal yr BP when the ice-patch $\delta^{18}O$ record indicated a return to milder conditions. Human activity paralleled increasing $\delta^{18}O$ until 1100 cal yr BP, after which it again rapidly declined coeval with warm temperatures, as indicated by ice-patch $\delta^{18}O$ and North American warmth associated with the Medieval Climate Anomaly (Trouet et al., 2013). Human activity since 1100 cal yr BP remained low, coinciding with isotopic values exceeding −18‰ for much of the last millennia.

The rapid increases in human activity leading to maxima at ca. 1200 and 4500 cal yr BP each corresponded to $\delta^{18}O$ values between −18 and −19‰, but abruptly ended when $\delta^{18}O$ exceeded −18‰, suggesting conditions surpassed a climatic threshold that no longer supported high levels of human activity in the region. Although other factors such as social patterns and cultural preferences influenced human activity, the close parallels with climate during the past 10,000 years suggest that climate extremes were likely an important influence on human activity in the region.

Data availability statement

All ice patch water isotope data are available at NOAA WDS Paleoclimatology archive at the following URL: https://www.ncdc.noaa.gov/paleo/study/31817.

Declaration of competing interest

The authors declare that they have no known competing financial interests or personal relationships that could have appeared to influence the work reported in this paper.

Acknowledgements

We thank U. Wisconsin Ice Drilling Design and Operations, M. Jayred for assistance in drilling the cores, and all of the project field and laboratory assistants. This project was funded by Buffalo Bill Historical Center's Draper Natural History Museum, University of Wyoming's Biodiversity Institute, Prince Albert II of Monaco Foundation—Monaco and USA, NSF grants BCS 1832486 and OPP 1925417, the U.S. Geological Survey Ecosystem Program and Climate Research and Development Program, INSTAAR, and the Sulo and Aileen Maki Endowment at the Desert Research Institute. Work on the Shoshone National Forest was conducted under permit #CFK317, and we thank Kyle Wright for his support. Any use of trade, firm, or product names is for descriptive purposes only and does not imply endorsement by the U.S. Government.

Appendix A. Supplementary data

Supplementary data to this article can be found online at https://doi.org/10.1016/j.qsa.2020.100021.

References

Anderson, L., 2011. Holocene record of precipitation seasonality from lake calcite $\delta^{18}O$ in the central Rocky Mountains, United States. Geology 39, 211–214.
Anderson, L., Abbott, M.B., Finney, B.P., Burns, S.J., 2005. Regional atmospheric circulation change in the North Pacific during the Holocene inferred from lacustrine carbonate oxygen isotopes, Yukon Territory, Canada. Quat. Res. 64, 21–35.
Anderson, L., Berkelhammer, M., Barron, J.A., Steinman, B.A., Finney, B.P., Abbott, M.B., 2016a. Lake oxygen isotopes as recorders of North American Rocky Mountain hydroclimate: Holocene patterns and variability at multi-decadal to millennial time scales. Global Planet. Change 137, 131–148.
Anderson, L., Berkelhammer, M., Mast, M.A., 2016b. Isotopes in North American Rocky mountain snowpack 1993-2014. Quat. Sci. Rev. 131, 262–273.
Beal, S.A., Osterberg, E.C., Zdanowicz, C.M., Fisher, D.A., 2015. Ice core perspective on mercury pollution during the past 600 years. Environ. Sci. Technol. 49, 7641–7647.
Benjamin, L., Knobel, L.L., Hall, L.F., Cecil, L.D., Green, J.R., 2004. Development of a local meteoric water line for southeastern Idaho, western Wyoming, and south-central Montana. U.S. Geological Survey Scientific Investigations, p. 17. Report 2004-5126.
Berger, W.H., 2010. On glacier retreat and drought cycles in the Rocky Mountains of Montana and Canada. Quat. Int. 215, 27–33.
Blaauw, M., Christen, J.A., 2011. Flexible paleoclimate age-depth models using an autoregressive gamma process. Bayesian Analysis 6, 457–474.
Brown, S.R., Stone, J.R., McLennan, D., Latimer, J., Westover, K.S., 2020. Landscape-lake interactions in the Beartooth Mountains, Wyoming: a 350-year fire history reconstruction. J. Paleolimnol. 64, 107–119.
Buntgen, U., Tegel, W., Nicolussi, K., McCormick, M., Frank, D., Trouet, V., Kaplan, J.O., Herzig, F., Heussner, K., Wanner, H., Luterbacher, J., Esper, J., 2011. 2500 Years of European climate variability and human susceptibility. Science 331, 578–582.
Carter, V.A., Shinker, J.J., Preece, J., 2018. Drought and vegetation change in the central Rocky Mountains and western Great Plains: potential climatic mechanisms associated with megadrought conditions at 4200 cal yr BP. Clim. Past 14, 1195–1212.
Chellman, N., McConnell, J.R., Arienzo, M., Pederson, G.T., Aarons, S.M., Csank, A., 2017. Reassessment of the Upper Fremont Glacier ice-core chronologies by synchronizing of ice-core-water isotopes to a nearby tree-ring chronology. Environ. Sci. Technol. 51, 4230–4238.
Craig, H., 1961. Isotopic variations in meteoric waters. Science 133, 1702–1703.
deMenocal, P.B., 2001. Cultural responses to climate change during the Late Holocene. Science 292, 667–673.
Denton, G.H., Porter, S.C., 1970. *Neoglaciation*. In: *Scientific American*, 222, pp. 100–111.
Dixon, J.L., Callanan, M.E., Hafner, A., Hare, P.G., 2014. The emergence of glacial archaeology. Journal of Glacial Archaeology 1, 1–9.
Fisher, D.A., Koerner, R.M., Paterson, W.S.B., Dansgaard, W., Gundestrup, N., Reeh, N., 1983. Effect of wind scouring on climatic records from ice-core oxygen-isotope profiles. Nature 301, 205–209.
Hall, M.H.P., Fagre, D.B., 2003. Modeled climate-induced glacier change in Glacier National Park, 1850-2100. Bioscience 53, 131–140.
Hare, P.G., Thomas, C.D., Topper, T.N., Gotthardt, R.M., 2012. The archaeology of Yukon ice patches: new artifacts, observations, and insights. Arctic 65, 118–135.
Hoffman, M.J., Fountain, A.G., Achuff, J.M., 2007. 20th-century variations in area of cirque glaciers and glacierets, Rocky Mountain National Park, Rocky Mountains, Colorado, USA. Ann. Glaciol. 46, 349–354.
Kelly, R.L., Surovell, T.A., Shuman, B.N., Smith, G.M., 2013. A continuous climatic impact on Holocene human population in the Rocky Mountains. Proc. Natl. Acad. Sci. U. S. A 110, 443–447.
Kuper, R., Kropelin, S., 2006. Climate-controlled Holocene occupation in the Sahara: motor of Africa's evolution. Science 313, 803–807.
Kuzyk, G.W., Russell, D.E., Farnell, R.S., Gotthardt, R.M., Hare, P.G., Blake, E., 1999. In pursuit of prehistoric caribou on Thandlat, southern Yukon. Arctic 52, 214–219.

Kyne, J., McConnell, J., 2007. The PrairieDog: a double-barrel coring drill for 'hand' augering. Ann. Glaciol. 47, 99–100.
Lee, C.M., 2018. Final Report – Continuing archaeological and paleobiological reconnaissance of perennial ice and snow patches, Custer Gallatin National Forest, Montana and Shoshone National Forest. INSTAAR, *Wyoming*.
Lee, C.M., 2010. Global warming reveals wooden artefact frozen over 10,000 years ago in the Rocky Mountains. Antiquity 325.
Lee, C.M., Puseman, K., 2017. Ice patch hunting in the Greater Yellowstone Area, Rocky Mountains, USA: wood shafts, chipped stone projectile points, and bighorn sheep (Ovis canadensis). Am. Antiq. 82, 223–243.
Liu, Z.F., Yoshimura, K., Bowen, G.J., Buenning, N.H., Risi, C., Welker, J.M., Yuan, F.S., 2014. Paired oxygen isotope records reveal modern North American atmospheric dynamics during the Holocene. Nat. Commun. 5, 3701.
Lundeen, Z., Brunelle, A., Burns, S.J., Polyak, V., Asmerom, Y., 2013. A speleothem record of Holocene paleoclimate from the northern Wasatch Mountains, southeast Idaho, USA. Quat. Int. 310, 83–95.
Marsicek, J., Shuman, B.N., Bartlein, P.J., Shafer, S.L., Brewer, S., 2018. Reconciling divergent trends and millennial variations in Holocene temperatures. Nature 554, 92–96.
Menounos, B., Osborn, G., Clague, J.J., Luckman, B.H., 2009. Latest Pleistocene and Holocene glacier fluctuations in western Canada. Quat. Sci. Rev. 28, 2049–2074.
Meulendyk, T., Moorman, B.J., Andrews, T.D., MacKay, G., 2012. Morphology and development of ice patches in Northwest Territories, Canada. Arctic 65, 43–58.
Naftz, D.L., Susong, D.D., Schuster, P.F., Cecil, L.D., Dettinger, M.D., Michel, R.L., Kendall, C., 2002. Ice core evidence of rapid air temperature increases since 1960 in alpine areas of the Wind River Range, Wyoming, United States. J. Geophys. Res.-Atmos. 107, 1–16.
Osborn, G., Karlstrom, E.T., 1988. Holocene history of the Bugaboo Glacier, British-Columbia. *Geology* 16, 1015–1017.
Overland, J.E., Adams, J.M., Bond, N.A., 1999. Decadal variability of the Aleutian low and its relation to high-latitude circulation. J. Clim. 12, 1542–1548.
Pederson, G.T., Gray, S.T., Woodhouse, C.A., Betancourt, J.L., Farge, D.B., Littell, J.S., Watson, E., Luckman, B.H., Graumlich, L.J., 2011. The unusual nature of recent snowpack declines in the North American cordillera. Science 333, 332–335.
Peros, M.C., Munoz, S.E., Gajewski, K., Viau, A.E., 2010. Prehistoric demography of North America inferred from radiocarbon data. J. Archaeol. Sci. 37, 656–664.
R Development Core Team, 2013. : A Language and Environment for Statistical Computing. R Foundation for Statistical Computing, Vienna, Austria, ISBN 3-900051-07-0. URL http://www.r-project.org.
Reckin, R., 2013. Ice patch archaeology in global perspective: archaeological discoveries from alpine ice patches worldwide and their relationship with paleoclimates. J. World PreHistory 26, 323–385.
Reimer, P.J., Bard, E., Bayliss, A., Beck, J.W., Blackwell, P.G., Ramsey, C.B., Buck, C.E., Cheng, H., Edwards, R.L., Friedrich, M., Grootes, P.M., Guilderson, T.P., Haflidason, H., Hajdas, I., Hatté, C., Heaton, T.J., Hoffmann, D.L., Hogg, A.G., Hughen, K.A., Kaiser, K.F., Kromer, B., Manning, S.W., Niu, M., Reimer, R.W., Richards, D.A., Scott, E.M., Southon, J.R., Staff, R.A., Turney, C.S.M., van der Plicht, J., 2013. IntCal13 and Marine13 radiocarbon age calibration curves 0-50,000 years cal BP. Radiocarbon 55, 1869–1887.
Salzer, M.W., Bunn, A.G., Graham, N.E., Hughes, M.K., 2014. Five millennia of paleotemperature from tree-rings in the Great Basin, USA. Clim. Dynam. 42, 1517–1526.
Shuman, B.N., Serravezza, M., 2017. Patterns of hydroclimatic change in the Rocky Mountains and surrounding regions since the last glacial maximum. Quat. Sci. Rev. 173, 58–77.
Shuman, B., Marsicek, J., 2016. The structure of Holocene climate change in mid-latitude North America. Quat. Sci. Rev. 141, 38–51.
Shuman, B., 2012. Recent Wyoming temperature trends, their drivers, and impacts in a 14,000-year context. Climatic Change 112, 429–447.
Solomina, O.N., Bradley, R.S., Hodgson, D.A., Ivy-Ochs, S., Jomelli, V., Mackintosh, A.N., Nesje, A., Owen, L.A., Wanner, H., C Wiles, G., Young, N.E., 2015. Holocene glacier fluctuations. Quat. Sci. Rev. 111, 9–34.
Stone, J.R., Saros, J.E., Pederson, G.T., 2016. Coherent late-Holocene climate-driven shifts in the structure of three Rocky Mountain lakes. Holocene 26, 1103–1111.
Thompson, L.G., Mosley-Thompson, E., Davis, M.E., Zagorodnov, V.S., Howat, I.M., Mikhatenko, V.N., Lin, P.N., 2013. Annually resolved ice core records of tropical climate variability over the past similar to 1800 years. Science 340, 945–950.
Trouet, V., Diaz, H.F., Wahl, E.R., Viau, A.E., Graham, R., Graham, N., Cook, E.R., 2013. A 1500-year reconstruction of annual mean temperature for temperate North America on decadal-to-multidecadal time scales. Environ. Res. Lett. 8, 024008.
United States Department of Agriculture (USDA). Natural Resources Conservation Services. Snow Telemetry (SNOTEL) and Snow Course Data and Products. Available at. www.wcc.nrcs.usda.gov/snow. (Accessed 9 April 2020).
Vachon, R.W., White, J.W.C., Gutmann, E., Welker, J.M., 2007. Amount-weighted annual isotopic ($\delta^{18}O$) values are affected by the seasonality of precipitation: a sensitivity study. Geophys. Res. Lett. 34, L21707.
Welker, J.M., 2012. ENSO effects on $\delta^{18}O$, $\delta^{2}H$ and d-excess values in precipitation across the U.S. using a high-density, long-term network (USNIP). Rapid Commun. Mass Spectrom. 26, 1893–1898.
Whitlock, C., Dean, W.E., Fritz, S.C., Stevens, L.R., Stone, J.R., 2012. Holocene seasonal variability inferred from multiple proxy records from Crevice Lake, Yellowstone National Park, USA. Palaeogeogr. Palaeoclimatol. Palaeoecol. 331–332, 90–103.
Wise, E.K., Woodhouse, C.A., McCabe, G.J., Pederson, G.T., St-Jacques, J.M., 2018. Hydroclimatology of the Missouri river basin. J. Hydrometeorol. 19, 161–182.
Yuan, F.S., Koran, M.R., Valdez, A., 2013. Late glacial and Holocene record of climatic change in the southern Rocky Mountains from sediments in San Luis Lake, Colorado, USA. Palaeogeogr. Palaeoclimatol. Palaeoecol. 392, 146–160.
Zahid, H.J., Robinson, E., Kelly, R.L., 2016. Agriculture, population growth, and statistical analysis of the radiocarbon record. Proc. Natl. Acad. Sci. U. S. A 113, 931–935.